Structural Variations in Pyrochlore-Structured $Bi_2Hf_2O_7$, $Bi_2Ti_2O_7$ and $Bi_2Hf_{2-x}Ti_xO_7$ Solid Solutions as a Function of Composition and Temperature by Neutron and X-ray Diffraction and Raman Spectroscopy

Stuart J. Henderson,[†] Olga Shebanova,[‡] Andrew L. Hector,*[,†] Paul F. McMillan,[‡] and Mark T. Weller[†]

School of Chemistry, University of Southampton, Southampton, United Kingdom, Department of Chemistry and Materials Chemistry Centre, University College London, 20 Gordon Street, London WC1H 0AJ, United Kingdom, and Davy−Faraday Research Laboratory, The Royal Institution of Great Britain, 21 Albemarle Street, London W1X 4BS, United Kingdom

Received December 3, 2006. Revised Manuscript Received February 6, 2007

The structural behavior of the pyrochlore $Bi_2Hf_2O_7$ with varying temperature has been studied by powder neutron diffraction X-ray diffraction, and Raman scattering. The unit cell undergoes phase changes that are determined by diffraction methods to occur between α-, *β*-, *γ*- and *δ*-polymorphs at around 400, 550 and 900 °C. The *δ*-$Bi_2Hf_2O_7$ polymorph corresponds to the ideal cubic pyrochlore phase. Three of the four polymorphs have previously been reported to occur for $Bi_2Sn_2O_7$. The need to accommodate the active Bi^{3+} lone pair in the presence of large HfO_6 octahedra results in an "icelike" ordering of Bi positions in $Bi_2Hf_2O_7$ at room temperature. A similar sequence of phase transitions is observed at room temperature with increasing Ti^{4+} for Hf^{4+} substitution in the compositional series $Bi_2Hf_{2-x}Ti_xO_7$. The structure changes as the space available to the Bi^{3+} ion increases represent a gradual increase in disorder and symmetry.

Introduction

Dielectric ceramics are widely used in microelectronics and microwave communication technologies.[1] Materials with high dielectric constants are particularly important in reducing the size of microelectronic circuits, in which high permittivity and low dielectric loss are required for many applications.[2] Bismuth-based pyrochlore compounds are attractive candidates for capacitor and high-frequency filter applications in multilayer structures cofired with silver electrodes.[3] Ternary oxide pyrochlores in the Bi_2O_3−ZnO−Nb_2O_5 (BZN) system have received intensive attention as they exhibit high dielectric constants (ϵ = 80−150), low dielectric losses, and chemically tunable temperature coefficients of capacitance (τ_c).[4,5] Tunability also exists for thin film samples according to the substrate used.[6] The variation in biaxial stress and tensile strain caused by varying the substrate can significantly influence the dielectric relaxation behavior of cubic BZN.[7] The utility of these pyrochlore type compounds is further enhanced by their low sintering temperatures (<950 °C).[8] Several experimental studies have been undertaken to further improve these properties, especially with regards to enhancing the permittivity and reducing dielectric loss. For example, substitution of Ti^{4+} into BZN materials resulted in a significant increase in dielectric constant with increasing titanium content.[1] Likewise, the dielectric constant of compounds in the $Bi_2Sn_{2-x}Ti_xO_7$ ($0 \leq x \leq 1.4$) system was found to increase almost linearly with increasing substitution of Ti^{4+}.[9]

The ideal cubic pyrochlore structure (Figure 1) crystallizes in the $Fd\bar{3}m$ space group. The structure is often described in terms of interpenetrating A_2O' and BO_6 networks, in which *A*, *B*, and O′ lie on special crystallographic positions. The position of the O atom (48*f*: *x*, $^1/_8$, $^1/_8$) varies according to the tilting of the BO_6 octahedra, the *B*−O distance and the coordination geometry around the *A* cation. Disorder in the A_2O' network is often seen when the A cation of a pyrochlore compound has an active lone pair. In the standard pyrochlore model, the *A* cation is located at the center of a puckered hexagonal ring of O atoms on a center of −3*m* symmetry. There are two short bonds equal in length to O′ along the 3-fold axis. A lone pair cannot easily be accommodated in this space. Avdeev has speculated that the disorder of *A* and O′ ions is present because of static displacements in most pyrochlore compounds in which the *A* cation has an active s^2 lone pair.[10] That this is likely to be the case has been supported by detailed studies on such compounds: for example, investigations of tin niobate and tantalate pyro-

* Corresponding author. Fax: 44 2380596805. Tel: 44 2380594125. E-mail: A.L.Hector@soton.ac.uk.
† University of Southampton.
‡ University College London and The Royal Institution of Great Britain.

(1) Du, H.; Yao, X. *Mater. Res. Bull.* **2005**, *40*, 1527
(2) Ling, H. C.; Yan, M. F.; Rhodes, W. W. *J. Mater. Res.* **1990**, *5*, 1752.
(3) Levin, I.; Amos, T. G.; Nino, J. C.; Vanderah, T. A.; Randall, C. A.; Lanagan, M. T. *J. Solid State Chem.* **2002**, *168*, 69.
(4) Kagata, H.; Inoue, T.; Kato, J.; Kameyama, I. *Jpn. J. Appl. Phys.* **1992**, *31*, 3152.
(5) Mergen, A.; Lee, W. E. *Mater. Res. Bull.* **1997**, *32*, 175.
(6) Lu, J.; Stremmer, S. *Appl. Phys. Lett.* **2003**, *83*, 2411.
(7) Lu, J.; Klenov, D. O.; Stremmer, S. *Appl. Phys. Lett.*, **2004**, *84*, 957.
(8) Zanetti, S. M.; da Silva, S. A.; Thim, G. P. *J. Solid State Chem.* **2004**, *177*, 4546.
(9) Takahashi, J.; Takatsu, M.; Ota, T.; Yamai, I. *J. Ceram. Soc. Jpn.* **1990**, *98*, 786.

10.1021/cm062864a CCC: $37.00
Published on Web 03/13/2007

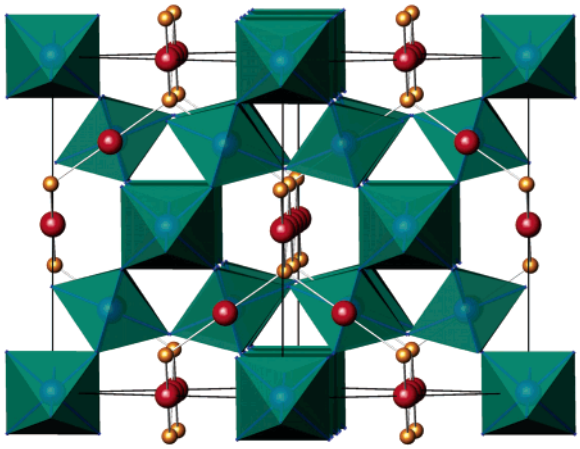

Figure 1. Ideal pyrochlore structure viewed along the (110) axis (*A* red, O′ orange, and BO_6 octahedra in green).

chlores using Mössbauer spectroscopy showed that the Sn^{2+} cations could not be located in the highly symmetric $-3m$ environment.[11] This was supported by observation of the 442 reflection in the powder X-ray diffraction pattern. In ideal cubic pyrochlores, this reflection is expected to have zero intensity. Its appearance could be rationalized by the presence of highly anisotropic thermal vibrations, or more successfully with a static displacement of the Sn^{2+} ions toward the surrounding ring of O atoms. This allows the lone pair to be accommodated with two or three of the Sn−O distances being shortened. Among analogous bismuth-containing pyrochlores, such disordering has been described by various mechanisms among systems with B = Ti,[12,13] Nb,[3] Ru,[10] or Sn.[14−16] The A_2O' network has also been compared with the crystal structure of ice-I_h. The Bernal−Fowler rules state that each O atom in the lattice is bonded tetrahedrally to four protons such that two are proximal (covalent) and two are distal (H-bonded).[17] In ice-I_h, these rules are not satisfied by any unique arrangement so that there is a residual zero-temperature entropy. Hence, it can be considered a structurally frustrated sytem.[18] Seshadri applied this analogy to compare the stereochemistry of the lone pairs of stoichiometric $Bi_2Ti_2O_7$ and the ferroelectric Aurivillius phase $SrBi_2Ta_2O_9$ using density functional calculations.[19]

In the room-temperature phase of $Bi_2Sn_2O_7$, disorder in the structure is very pronounced. This highly complex structure has only recently been solved by simulated annealing methods.[20] The average displacements from the ideal pyrochlore sites for Bi, Sn, O, and O′ were calculated to be 0.389, 0.104, 0.189, and 0.312 Å, respectively. This highlights the greater distortion of the Bi−O′ sublattice compared to that of the corresponding Sn−O case. At 140 °C, a transformation occurs to a face-centered cubic unit cell with dimensions that are doubled relative to those of a standard pyrochlore ($a = 21.4$ Å). Kennedy suggested that this phase could be refined in the space group $F43c$ and that there was an ordered displacement of the Bi atoms.[14] However, no structural model was provided in that work. Above 630 °C, $Bi_2Sn_2O_7$ achieves a standard face-centered cubic pyrochlore structure ($a = 10.75$ Å), but with disorder occurring at the bismuth site similar to that found in $Bi_2Ti_2O_7$[13] and BZN.[3] The Bi is displaced to a 96 fold site with the O′ having a large thermal parameter.[16]

The preparation of $Bi_2Hf_2O_7$ was first described by Sleight, and diffraction experiments indicated that the compound was isostructural with $Bi_2Sn_2O_7$.[21] A recent study[22] showed that BZN and its tantalate (BZT) or stibate (BZS) analogues exhibit a strong correlation between the Bi^{3+} off-center displacement and the dielectric constant. The recent solution of the stannate structure,[20] and our own recent finding of large Bi site displacements in $Bi_2Ti_2O_7$,[13] prompted us to revisit bismuth hafnate and its solid solution with bismuth titanate pyrochlore.

Experimental Section

$Bi_2Hf_2O_7$ was prepared following the literature procedure,[21] as were $Bi_2Ti_2O_7$[13] and $Bi_2Sn_2O_7$.[20] $Bi_2Hf_{2-x}Ti_xO_7$ ($0.2 \le x \le 1.8$) samples were prepared by coprecipitation of a basic titanium solution with an acidic bismuth/hafnium solution in the appropriate stoichiometric ratio. Titanium (−100 mesh) was added to a mixture of hydrogen peroxide (28%, 40 mL) and ammonia solution (35%, 14 mL). The stirred mixture was maintained at just below room temperature using a water bath and the titanium dissolved over a period of 3−4 h, resulting in a bright yellow solution. This was added quickly to a stirred solution of bismuth nitrate pentahydrate and hafnium oxynitrate hydrate in 1.2 mol dm^{-3} HNO_3 (50 cm^3). Initially, a dark orange solution formed with vigorous evolution of gas. With continued stirring, a pale cream precipitate soon formed; this was stirred for 30 min to agglomerate the particles and ensure complete precipitation. After filtering and washing with dilute (10%) ammonia, we dried the cream-colored solid at 50 °C. To minimize loss of bismuth through volatilization, we calcined samples as pressed disks. These were stacked in a closed alumina crucible before firing for 16 h at temperatures as high as the stability of each phase permitted (470 °C for $Bi_2Ti_2O_7$,[13] 500 °C for $x = 1.8$, 550 °C for $x = 1.6$, 600 °C for $x = 1.4-0.6$, 700 °C for $x = 0.4-0.2$, and 875 °C $Bi_2Hf_2O_7$). Although it was previously reported[21] that $Bi_2Hf_2O_7$ was formed at up to 950 °C, thermogravimetric analysis indicated weight loss above 875 °C. Analyses of samples fired above this temperature revealed the presence of an HfO_2 impurity.

Powder X-ray diffraction (PXD) patterns were collected using a Siemens D5000 diffractometer. Variable temperature PXD was carried out using a Bruker D8 Advance diffractometer fitted with an Anton Paar HTK-1200 high-temperature furnace. Both instruments employed Cu$K_{\alpha 1}$ radiation. Powder neutron diffraction (PND) data for $Bi_2Hf_2O_7$ were collected using the high-resolution time-of-flight HRPD diffractometer at the ISIS facility. The 3 g sample

(10) Avdeev, M.; Haas, M. K.; Jorgensen, J. D.; Cava, R. J. *J. Solid State Chem.* **2002**, *169*, 24.
(11) Birchall, T.; Sleight, A. W. *J. Solid State Chem.* **1975**, *13*, 118.
(12) Radosavljevic, I.; Evans, J. S. O.; Sleight, A. W. *J. Solid State Chem.* **1998**, *136*, 63.
(13) Hector, A. L.; Wiggin, S. B. *J. Solid State Chem.* **2004**, *177*, 139.
(14) Kennedy, B. J.; Ismunandar, Elcombe, M. M. *Mater. Sci. Forum* **1998**, *278−281*, 762.
(15) Shannon, R. D.; Bierlein, J. D.; Gillson, J. L.; Jones, G. A.; Sleight, A. W. *J. Phys. Chem. Solids* **1980**, *41*, 117.
(16) Jones, R. H.; Knight, K. S. *J. Chem. Soc., Dalton Trans.* **1997**, 2551.
(17) Bernal, J. D.; Fowler, R. H. *J. Chem. Phys.* **1933**, *1*, 515.
(18) Pauling, L. *J. Am. Chem. Soc.* **1935**, *57*, 2680.
(19) Seshadri, R. *Solid State Sci.* **2006**, *8*, 259.
(20) Radosavljevic Evans, I.; Howard, J. A. K.; Evans, J. S. O. *J. Mater. Chem.* **2003**, *13*, 2098.
(21) Sorokina, S. L. Sleight, A. W. *Mater. Res. Bull.* **1998**, *33*, 1077.
(22) Melot, B.; Rodriguez, E.; Proffen, T.; Hayward, M. A.; Seshadri, R. *Mater. Res. Bull.* **2006**, *41*, 961.

was mounted in a sealed silica tube (7 mm O/D) placed inside a vanadium can (8 mm O/D) at 22, 600, and 950 °C. Data from the backscattering bank ($2\theta = 168.33$ °) with a time-of-flight range of 40−120 μs ($d = 0.828$−2.484 Å) were analyzed using the GSAS package.[23] Similarly, the PXD data for the $Bi_2Hf_{2-x}Ti_xO_7$ series were refined, though here the oxygen sites were not refined because of their weak scattering ability.

Raman spectra were obtained using a custom-built microbeam instrument.[24] Raman scattering was excited with the 514.5 nm line of an air-cooled 50 mW Ar^+ laser, focused onto the sample using a long-working distance Mitutoyo 50SL objective. The backscattered signal was collected through the same objective. A table-top confocal setup including Kaiser SuperNotch filters was used to discriminate the incident laser light scattering from the Raman signal. The spectra were obtained using a 500 mm Acton 300 spectrometer and a liquid N_2-cooled back-illuminated Si CCD detector. Some high-temperature spectra were obtained using a commercial InVia Renishaw spectrometer system. Low- and high-temperature Raman measurements were performed using a TS1500 Stage from Linkam Scientific Instruments Ltd. During the low-temperature runs, pressed discs of sample were placed directly on the silver plate surface to ensure accurate temperature readings. For high-temperature measurements, samples were placed on a quartz disk contained within the enclosed high-*T* furnace chamber.

Thermal analyses were carried out using a Polymer Laboratories STA 1500 between 25 and 1000 °C under flowing air. Samples were also analyzed by EDX using a Jeol JSM-5910 with an Oxford Inca 300 detector. Area scans on pressed pellets showed the expected Bi:Hf:Ti ratios within experimental error. Dielectric measurements were performed with a Solartron SI 1260 Impedance/gain-phase analyzer and 1296 Dielectric Interface at frequencies in the range of 1 kHz to 1 MHz on silver-plated pressed pellets. Dielectric constants were obtained within the expected[25,26] range ($\epsilon_0 \approx 52$−149) for these materials, but systematic changes could not be observed. Cold or warm (2 kB, 300 °C) pressing of these samples resulted in only about 80% of the theoretical density, and another densification method will be required to allow accurate determination of the dielectric properties.

Results

$Bi_2Hf_2O_7$. Inspection of the room-temperature PXD data suggested that $Bi_2Hf_2O_7$ is indeed isostructural with $Bi_2Sn_2O_7$. Variable temperature PXD data were recorded in 50 °C steps up to 900 °C to compare the phase behavior of $Bi_2Hf_2O_7$ with $Bi_2Sn_2O_7$. Three distinct phase transitions were identified at around 400, 550, and 900 °C (Figure 2). $Bi_2Sn_2O_7$ has been reported[14] to exhibit two transitions at 90 °C (α−β) and 680 °C (β−γ). The $Bi_2Hf_2O_7$ diffraction pattern above 550 °C was not consistent with a doubled cubic cell but exhibited more reflections than the standard $Fd\bar{3}m$ pyrochlore model allows. The 900 °C phase was consistent with a standard pyrochlore, though no intensity was seen for the 311 reflection. High-resolution PND experiments, in sealed silica tubes to prevent Bi loss, were undertaken to fully investigate these phases in more detail.

α-$Bi_2Hf_2O_7$ (22 °C). The room-temperature structure of $Bi_2Sn_2O_7$ was unknown for many years because of the complexity of its unit cell. Using simulated annealing methods, the structure was recently solved in the P_c space group with 176 crystallographically independent atoms.[20] The structure of $Bi_2Hf_2O_7$ was refined using this as a starting model. Initially lattice parameters and thermal parameters (with like atoms constrained together) were refined. Because of the low sintering temperature, peaks were broader than those used in refinements on $Bi_2Sn_2O_7$. It was not possible to simultaneously refine all atom positions freely to convergence. However, using soft constraints on the Hf−O, O−O, and Bi−O′ bond lengths and a high level of damping on the atom positions produced a stable refinement. The soft constraint distances were obtained by an iterative process, the Hf−O and Bi−O′ (each Bi having one short and one long bond to O′) distances were regularly reset to their average value, and O−O was set as $\sqrt{2}\times$ the Hf−O distance to maintain a roughly octahedral geometry. With refinement of the peak shape profiles, background, and a linear absorption correction ($\mu_R = 57$ cm^{-1}), a good fit was achieved to the data ($R_p = 4.16\%$, $R_{wp} = 4.65\%$, and $\chi^2 = 1.79$) with sensible bond lengths and angles. The O′ thermal parameter was slightly high, which may have indicated an oxygen deficiency, refining the O′ occupancy gave a value of 0.95. However, there was no indication of Bi or Hf deficiency and lower oxidation states than those of Bi^{3+} and Hf^{4+} are unlikely considering the synthesis method, so the occupancy of O′ was retained as unity in the final model. The final lattice parameters were $a = 15.3536(4)$ Å, $b = 15.3320(4)$ Å, $c = 21.8253(3)$ Å, and $\beta = 90.051(5)$°.

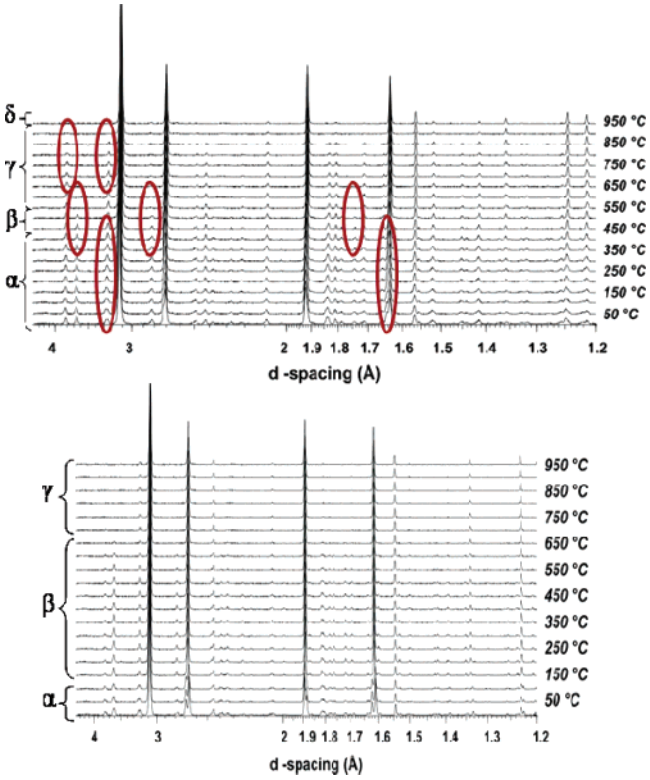

Figure 2. Variable temperature X-ray diffraction patterns of $Bi_2Hf_2O_7$ (top) and $Bi_2Sn_2O_7$ (bottom) showing the phase transitions with temperature. Note that δ-$Bi_2Hf_2O_7$ is isostructural with γ-$Bi_2Sn_2O_7$.

***β*-$Bi_2Hf_2O_7$ (450 °C).** This phase was not observed in the initial X-ray study due to its similarity to the γ-phase. However, detailed VT−PXD experiments showed that

(23) Von Dreele, R. B.; Larson, A. C. *GSAS General Structure Analysis System*; Neutron Scattering Center, MS-H805, Los Alamos National Laboratory: Los Alamos, NM, 2001.
(24) Soignard, E.; McMillan, P. F. *Chem. Mater.* **2004**, *16*, 3533.
(25) Huiling, D. Xi, Y. *J. Mater. Sci.: Mater. Electron.* **2004**, *15*, 613.
(26) Valant, M.; Davies, P. K. *J. Am. Ceram. Soc.* **2000**, *83*, 147.

Table 1. Two Possible Pyrochlore Models for γ-$Bi_2Hf_2O_7$

$I4_122$ (No. 98)					$I\bar{4}m2$ (No.119)				
Bi	8*f*	1/4	$-x + 1/2 \approx 0$	3/8	Bi	8*i*	$x \approx 1/4$	0	$z \approx 3/8$
Hf	8*f*	1/4	$x \approx 0$	7/8	Hf	8*i*	$x \approx 1/4$	0	$z \approx 7/8$
O	8*d*	*x*	$-x$	0	O	8*g*	*x*	*x*	0
	8*e*	$-x$	x	0		8*h*	*x*	$x+1/2$	1/4
	8*c*	0	0	*z*		4*e*	0	0	*z*
O′	4*b*	0	0	1/2		4*f*	0	1/2	*z*
					O′	2*b*	0	0	1/2
						2*d*	0	1/2	3/4

transformation to a face-centered cubic cell, as in the stannate, occurs at around 400 °C. No model has yet been described for β-$Bi_2Sn_2O_7$, but it has been indexed on the basis of a large cubic cell with $a = 21.45$ Å. This is approximately double that of a standard pyrochlore and a $\sqrt{2}a\times$ multiple of the α-phase. Systematic absences suggested a possible space group of $F\bar{4}3c$.[14] Indexing and Lebail extractions of our short neutron collections and X-ray data of $Bi_2Hf_2O_7$ at 450 °C were consistent with these findings. The lattice parameter was refined to $a = 21.733(2)$ Å.

γ-$Bi_2Hf_2O_7$ (600 °C). The PND data contained reflections and peak splitting that required a distortion of the unit cell away from the ideal cubic pyrochlore. Model independent refinements were carried out using the space groups from the $Fd\bar{3}m$ subgrouping as described by Hiroi.[27] The subgrouping follows reductions in the pyrochlore symmetry from a cubic face-centered to a tetragonal body-centered lattice. It was clear that the phase was tetragonal, as the difference between the *a* and *c* parameters was significantly greater than the statistical error ($\sqrt{2}a/c = 1.002$). The space group $I4_1/amd$ could be ruled out, as it did not allow the reflection at $d = 1.51$ Å to be modeled. The remaining possibilities all had similar fit statistics from Lebail extractions. Examination of the literature revealed two models (space groups $I\bar{4}m2$ and $I4_122$) that could be used for comparative Reitveld refinement of the data. Table 1 shows the atomic positions for the two models. The position of the Bi and Hf sites are described by 8 fold sites in both space groups. For $I4_122$, the O positions are described by three 8-fold sites and a 4-fold O′ site. The lower symmetry $I\bar{4}m2$ model requires two 2-fold O′ sites with two 8-fold and two 4-fold positions to describe O. In a translation from $I4_122$ to I-4*m*2 a 2-fold axis is removed and a mirror plane added. Both models gave a reasonable fit to the data, but the fit statistics were slightly better for the $I4_122$ model than the $I\bar{4}m2$ ($R_p = 4.63$ and 4.82%, respectively). As the extra oxygen positions did not improve the description of the structure, the lower symmetry $I\bar{4}m2$ model was discounted.

Anisotropic refinement of the bismuth atom in the $I4_122$ model resulted in an unusual elongated ellipsoid extending perpendicularly away from the Bi−O′ bond. The unusual shape of the Bi ellipsoid suggested that a split Bi position may be required to more accurately describe the site. The only available site with lower symmetry than the 8*f* (1/4, $-x + 1/2$, 3/8) is the 16*g* (*x*, *y*, *z*) site. Displacement to this site was tested with an appropriate reduction in the occupancy. The refinement proceeded smoothly and gave a slight improvement in the fit as well as more reasonable

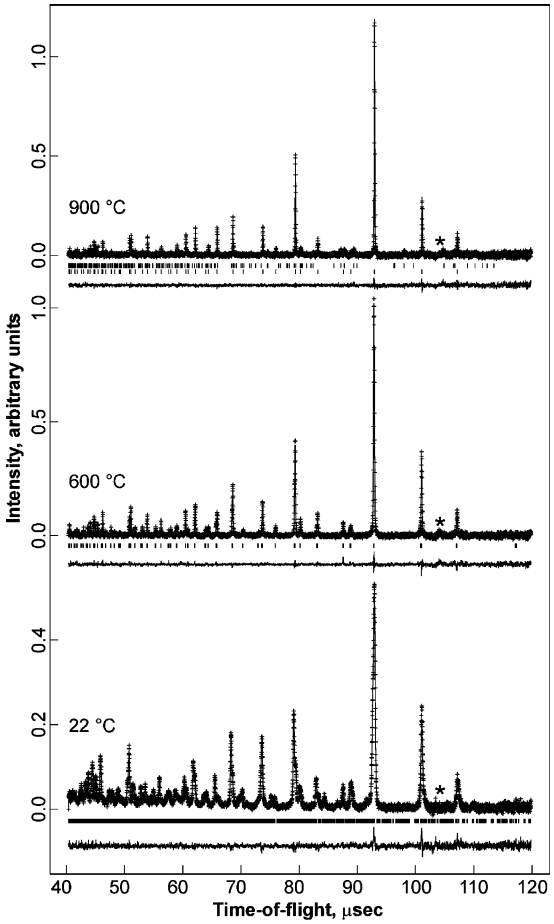

Figure 3. Final fits to PND data for $Bi_2Hf_2O_7$. In each case, crosses mark the data points, the upper continuous line the calculated profile and the lower continuous line the difference. Tick marks indicate the positions of the reflections; in the 900 °C pattern, the upper set of tick marks indicate the HfO_2 impurity. Asterisks mark the position of the main peak due to the vanadium sample can. The 900 °C pattern is fitted with Bi placed on the 96*g* site, but an identical fit is obtained with the 96*h* position.

thermal parameters for Bi (with U_{iso} falling to 0.014 from 0.047 Å^2). The thermal ellipsoid of the O′ atom was a large disk shape, the edges of which extended toward the side of the puckered ring not occupied by the bismuth, suggesting some disorder. A split site was tested, moving O′ to an 8*c* (0, 0, *z*) site and halving the occupancy. More reasonable thermal parameters were obtained, but the statistical fit was slightly worse than that achieved with an anisotropic 4-fold site ($\chi^2 = 1.546$ vs 1.535); hence, the split site was discounted. Figure 3 shows the final fit to the data and Table 2 shows the refined crystallographic parameters for γ-$Bi_2Hf_2O_7$.

δ-$Bi_2Hf_2O_7$ (900 °C). Preliminary refinements were carried out using the ideal pyrochlore structure (Bi (0,0,0), Hf (1/2, 1/2, 1/2), O (x, 1/8, 1/8) and O′ (1/8, 1/8, 1/8)) in the $Fd\bar{3}m$ space group, with isotropic temperature factors on all atoms except O. A minor HfO_2 impurity was included in the refinement using the monoclinic model appropriate for this temperature.[28] The loss of Bi through volatilization should be minimized by the sealed quartz tube in which the sample was mounted; however, a small amount of decomposition

(27) Yamaura, J. I.; Hiroi, Z. *J. Phys. Soc. Jpn.* **2002**, *71*, 2598.

(28) Hann, R. E.; Suitch, P. R.; Pentecost, J. L. *Phase Trans.* **1992**, *38*, 127.

Table 2. Refined Crystallographic Parameters for γ-$Bi_2Hf_2O_7$ at 600 °C[a]

atom	*x*	*y*	*z*	U_{11}	U_{22}	U_{33}	U_{12}	U_{13}	U_{23}
Bi	0.2215(8)	0.0366(4)	0.3524(3)	3.21(13)	3.21	3.21	0	0	0
Hf	1/4	−0.0022(3)	7/8	3.70(21)	0.01(12)	1.94(15)	0	1.34(10)	0
O1	0.1997(4)	0.1997(4)	0	4.83(20)	4.83(20)	4.90(41)	1.75(21)	3.18(16)	−3.18(16)
O2	−0.1965(4)	0.1965(4)	0	4.07(22)	4.07(22)	4.99(45)	2.32(24)	−1.09(15)	−1.09(15)
O3	0	0	0.1999(3)	6.06(41)	5.36(36)	4.97(27)	−3.74(32)	0	0
O′	0	0	1/2	3.74(24)	3.74(24)	11.55(52)	−3.32(37)	0	0

[a] Space group $I4_122$, $a = 7.68966(3)$ Å, $c = 10.85169(8)$ Å, $\chi^2 = 1.535$, $R_{wp} = 4.85\%$, $R_p = 4.12\%$. Estimated standard deviations are given in parentheses and thermal displacement parameters are in units of Å$^2 \times 100$.

Table 3. Refined Crystallographic Parameters for δ-$Bi_2Hf_2O_7$ at 900 °C.[b]

atom	*x*	*y*	*z*	occupancy	U_{11}	U_{22}	U_{33}	U_{12}	U_{13}	U_{23}
Bi	−0.0166(9)	−0.0166(9)	0.0300(8)	0.16667	2.52(16)	2.52	2.52	0	0	0
Hf	1/2	1/2	1/2	1	2.20(10)	2.20	2.20	0	0	0
O1	0.4246(2)	1/8	1/8	1	5.67(18)	0	0	4.41(11)	−2.39(8)	4.41(11)
O2	1/8	1/8	1/8	1	8.41(24)	8.41	8.41	0	0	0

[b] Space group $Fm\bar{3}m$, $a = 10.87791(3)$ Å, $\chi^2 = 1.131$, $R_{wp} = 5.80\%$, $R_p = 5.10\%$. Estimated standard deviations are given in parentheses and thermal displacement parameters are in units of Å$^2 \times 100$. Monoclinic HfO_2 was refined as a second phase with a refined phase fraction (corrected for cell volume) of 11%.

clearly occurred. TGA experiments under flowing air showed weight loss from around 870 °C. The remaining weak reflections at 2.15, 1.51, and 1.23 Å were attributed to the vanadium sample holder. A reasonable fit to the data was obtained but with very high thermal parameters on the Bi and O′ ($U_{iso} = 0.1074$ and 0.0814 Å^2). Anisotropic refinement of the Bi thermal parameter improved the fit further ($R_p = 5.35$ vs 5.14%) and gave intensity to the previously zero-intensity 442 reflection ($d = 1.813$ Å). Broadening of the Bi thermal ellipsoid perpendicular to the [111] axis, toward the puckered ring of O atoms occurred. This indicated that a static displacement of the Bi to a 96*g* (*x*, *x*, *z*) or 96*h* (0, *y*, −*y*) site as in $Bi_{1.74}Ti_2O_{6.62}$,[12] $Bi_2Ti_2O_7$,[13] and γ-$Bi_2Sn_2O_7$[17] could be a better structural representation. These sites both correspond approximately to a ring of scattering density around the central bismuth site. The displacement of the Bi was toward the center of each pair of O atoms (96*g*) or toward each O atom in the puckered ring (96*h*). Refinements using either of these positions resulted in identical fit statistics, with a slight improvement ($\chi^2 = 1.13$ vs 1.23) over the description of Bi with anisotropic thermal parameters. Both displacements gave more reasonable bismuth thermal parameters ($U_{iso} = 0.025$ Å^2).

The possibility of positional disorder about the O′ site was then tested, as its thermal parameter remained high after displacement of the Bi atom. Such disorder can be achieved using several possible sites. O′ is located at the center of a tetrahedron formed by the ideal bismuth sites. A displacement toward or away from each vertex of the tetrahedron can be described using the 32*e* (*x*, *x*, *x*) site.[10,14] The 48*f* (x,1/8,1/8) site will displace O′ toward the center of each edge of the tetrahedron. The 96*g* and 96*h* sites will displace O′ roughly toward half of the bismuth sites as described by the 96*g* Bi displacement.[3] Refinements were carried out with the O′ displaced to each of these sites with both possible Bi positions. Initially, a reduced thermal parameter was found in all cases, but refinement of the atom position tended toward the central site with a very high thermal parameter. Modeling the O′ with a combination of the 8*a* and 32*e* site as described for $Bi_2Ti_2O_7$[13] also resulted in no improvement in the fit, and refinements were unstable. Exploration of the O′ site using δF_{hkl} Fourier maps indicated that the nuclear density around the site is purely spherical. The large observed thermal parameter can thus be considered as resulting from thermal motion at the high measurement temperature or to disordered displacements of O′; there is no evidence for any static displacement. The final fit achieved to the data is shown in Figure 3 and refined parameters are presented in Table 3.

Table 4. Refined Structural Parameters for the $Bi_2Hf_{2-x}Ti_xO_7$ ($0 \le x \le 2$) Series[c]

x	space group	*a* (Å)	*b* (Å)	*c* (Å)	β (deg)	*V* (Å^3)
0	P_c	15.357(1)	15.341(1)	21.849(1)	90.04(1)	5147(1)
0.2	P_c	15.283(2)	15.255(2)	21.681(2)	90.03(2)	5055(1)
0.4	P_c	15.191(3)	15.159(3)	21.560(4)	89.72(1)	4962(2)
0.6	$I4_122$	7.5487(7)	7.5487(7)	10.716(2)	90	610.6(1)
0.8	$I4_122$	7.473(2)	7.473(2)	10.622(6)	90	593.2(4)
1	$I4_122$	7.469(2)	7.469(2)	10.606(4)	90	591.6(3)
1.2	$I4_122$	7.434(2)	7.434(2)	10.577(4)	90	584.5(3)
1.4	$I4_122$	7.422(1)	7.422(1)	10.558(3)	90	581.6(2)
1.6	$I4_122$	7.3897(9)	7.3897(9)	10.532(2)	90	575.1(2)
1.8	$I4_122$	7.3555(6)	7.3555(6)	10.446(1)	90	565.2(1)
2.0	$Fd\bar{3}m$	10.382(1)	10.382(1)	10.382(1)	90	1119.0(2)

[c] Estimated standard deviations are in parentheses.

$Bi_2Hf_{2-x}Ti_xO_7$. Phase identification of the $Bi_2Hf_{2-x}Ti_xO_7$ ($0 \le x \le 2$) series revealed a trend in compositional variation similar to that observed with temperature in $Bi_2Hf_2O_7$. Structures were refined from PXD data, so structural analysis was limited to identifying which structure type was present and refining for lattice parameters. As the titanium content is increased, the structure changes from that of α- to γ- and then δ-$Bi_2Hf_2O_7$, Table 4. An analogue of β-$Bi_2Hf_2O_7$ is not observed in this system. Lattice parameters given in Table 3 for $Bi_2Hf_2O_7$ and $Bi_2Ti_2O_7$ are from the PXD refinements analyzed in the same way as those of the solid solutions, thus they vary slightly from those derived by fitting of the PND data herein and reported previously.[13] It is interesting to note that the temperature at which these phases crystallize also varies with composition. Stoichiometric bismuth titanate has previously been shown to form only at 470 °C,[13] whereas bismuth hafnate can be prepared between 700 and 875 °C. The synthesis temperature for the intermediate phases increases as the titanium content decreases.

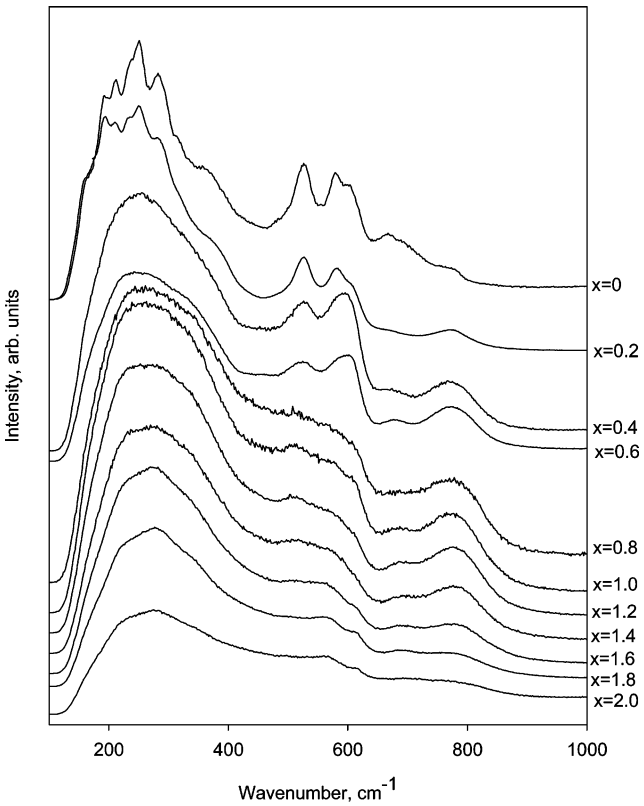

Figure 4. Raman spectra collected from samples in the $Bi_2Hf_{2-x}Ti_xO_7$ series at room temperature.

The phases observed in $Bi_2Hf_{2-x}Ti_xO_7$ were not reported in a previous study of $Bi_2Sn_{2-x}Ti_xO_7$ ($0 \leq x \leq 1.4$).[9] However, accurate structures of $Bi_2Sn_2O_7$[20] and $Bi_2Ti_2O_7$[13] were not known at the time of that work. Instead, a transition was observed at $x = 0.6$ from the α-$Bi_2Sn_2O_7$ structure (described as tetragonal) to a large cubic cell β-$Bi_2Sn_2O_7$ type structure. Further investigation of the Sn−Ti system may show a closer analogy to the phase behavior observed in the Hf−Ti system in this work.

Raman Spectra of $Bi_2Hf_2O_7$ and $Bi_2Hf_{2-x}Ti_xO_7$. The room-temperature (unpolarized) Raman spectrum of polycrystalline $Bi_2Hf_2O_7$ contains sharp peaks sitting on top of a series of broad bands in the 200−400, 450−650, and 650−800 cm^{-1} regions (Figure 4). The spectra are similar to data obtained for perovskite oxide samples containing highly polarizable metal ions, such as (Ba,Sr,Pb)(Ti,Nb,Pb,Zr)O_3, etc.[29−35] The origins of the sharp peaks vs broad features have been discussed at length for the perovskites. The broadest bands are due to: (a) second-order Raman scattering associated with the large electronic polarizibility of the transition metal and lone-pair or Jahn−Teller active (Pb^{2+}, Bi^{3+}, Nb^{5+}) ions; (b) disorder-induced first-order scattering mainly away from the Brillouin zone center, which can be associated with either chemical substitution or electronic effects driving off-center displacements of the cations; (c) a combination of these effects.[31,36] The sharp peaks arise because of symmetry-allowed first-order Raman scattering that can appear due to lattice distortions and descent in symmetry from an ideal structure, often accompanied by an increase in the unit-cell size. To further complicate the interpretation of the spectra, "sharp" first-order peaks can be substantially broadened by electron−phonon coupling that reduces the lifetime of excited vibrational states. Also, normally IR-active features can be observed in the Raman spectra because of symmetry-breaking due to static and dynamic disorder effects that cause relaxation of the normal selection rules. From the above, it can be said that (i) the local symmetries and phase transitions deduced from Raman scattering may not correspond exactly to those indicated by analysis of neutron or X-ray diffraction data, but (ii) the Raman spectra may contain additional information on local ordering and dynamic processes that may be difficult to extract from the diffraction studies.

Within perovskites and pyrochlores, symmetry descent and unit-cell changes among pure compounds are often reflected in second-order displacive phase transitions accompanied by soft modes occurring at special points within the Brillouin zone (e.g., at the zone edge, along particular directions, to give rise to transitions that augment the unit cell dimensions). These phase transitions occur as a function of varying the temperature or pressure.[32,34,35,37−39] Symmetry transitions can also occur as a function of chemical substitution along a solid solution series, as the average size of the cation occupying a given site is changed. In such cases, chemical disordering can also result in peak broadening, or new lattice symmetries can arise because of local or long-range ordering, resulting in new sets of Raman active modes.

The ideal cubic pyrochlore structure as exemplified by $Bi_2Ti_2O_7$ belongs to space group $Fd\bar{3}m$ (O_h^7) and contains $Z = 8$ formula units. Symmetry analysis indicates that the zone-center vibrational modes correspond to

$$\Gamma_{vib} = A_{1g}(R) + E_g(R) + 4F_{2g}(R) + 7F_{1u}(IR) + 3A_{2u}(i.a.) + 3E_u(i.a.) + 2F_{1g}(i.a.) + 4F_{2u}(i.a.)$$

where R or IR denotes Raman vs IR optical activity, and i.a. denotes inactive modes. In addition, the acoustic mode (F_{1u} symmetry) is present at the cubic zone center.

Despite the expected rich set of six peaks predicted by the symmetry analysis ($A_{1g} + E_g + 4F_{2g}$), the Raman spectrum of $Bi_2Ti_2O_7$ shows only broad features at 250−400, 450−620, and 640−870 cm^{-1}, which are "decorated" with various shoulders and weak sharper features. From previous studies on vibrational modes in metal oxide perovskites and pyrochlores, the highest-frequency features are associated with octahedral metal−oxygen stretching vibrations, the midrange vibrational modes are due to bending

(29) Gillet, P.; Guyot, F.; Price, G. D.; Tournerie, B.; Le Cleach, A. *Phys. Chem. Miner.* **1993**, *20*, 159.
(30) McMillan, P. F.; Ross, N. L. *Phys. Chem. Miner.* **1988**, *16*, 21.
(31) Perry, C. H.; Fertel, J. H.; and McNelly, T. F. *J. Chem. Phys.* **1967**, *47*, 1619.
(32) Perry, C. H.; Hall, D. B. *Phys. Rev. Lett.* **1965**, *15*, 700.
(33) Taylor, W.; Murray, A. F. *Solid State Commun.* **1979**, *31*, 937.
(34) Fontana, M. D.; Idrissi, H.; Kugel, G. E.; Wojcik, K. *J. Phys. Cond. Mater.* **1991**, *3*, 8695.
(35) Fleury, P. A.; Scott, J. F.; Worlock, J. M. *Phys. Rev. Lett.* **1968**, *21*, 16.
(36) Nilsen, W. G.; Skinner, J. G. *J. Chem. Phys.* **1968**, *48*, 2240.
(37) Cowley, R. A. *Phys. Rev.* **1964**, *134*, A981.
(38) Starykh, O. A.; Furusaki, A.; Balents, L. *Phys. Rev. B* **2005**, *72*, 094416.
(39) Knee, C. S.; Holmlund, J.; Andreasson, J.; Käll, M.; Eriksson, S. G.; Börjesson, L. *Phys. Rev. B* **2005**, *71*, 214518.

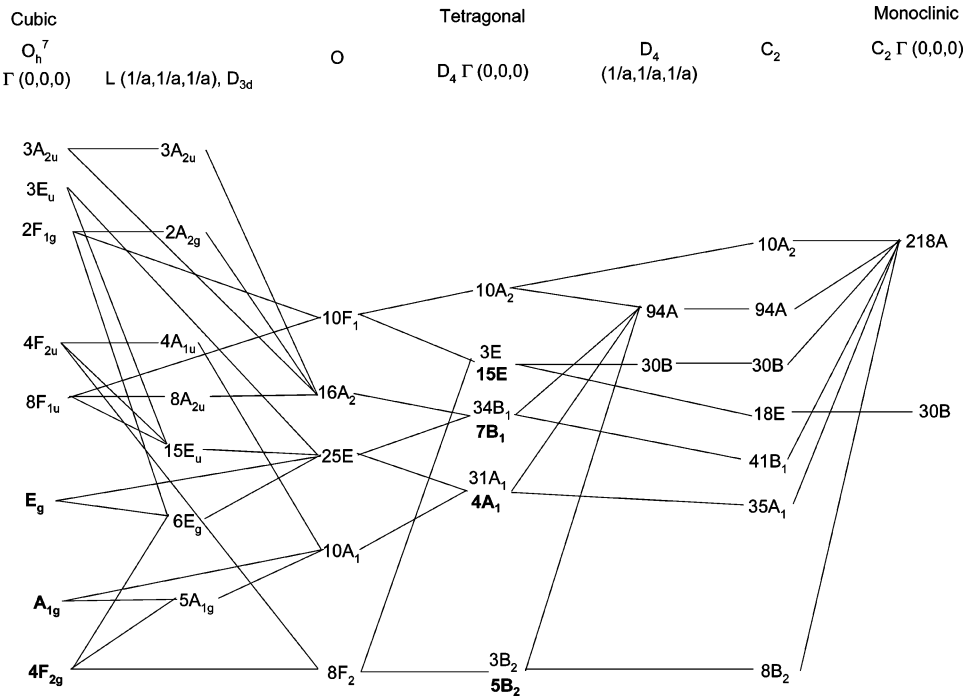

Figure 5. Correlation analysis for the subsequent phase transformations of $Bi_2Hf_2O_7$ from the cubic structure to the tetragonal unit cell and monoclinic unit cell. Raman active modes are shown in bold. Correlation tables are used from Decius and Hexter.[40]

modes of the MO_6 octahedra, and the lowest-frequency vibrations are due to large cation displacements combined with octahedral deformations. The broad features in the spectrum of $Bi_2Ti_2O_7$ are mainly due to second-order scattering combined with dynamically induced first-order scattering due to the large electronic polarizibility of the metal ions and electron−phonon coupling effects, thus reflecting the approximate vibrational density of states within the sample.

In the case of the Raman spectrum of $Bi_2Hf_2O_7$ recorded at room temperature, many more sharp features are present in the spectrum. These indicate a considerably lowered symmetry and expanded unit cell. The crystal structure has a very large, low-symmetry unit cell. It is obvious that such a low-symmetry cell should contain a very large number of zone-center Raman active peaks. We have carried out a descent in symmetry analysis (Figure 5) through various pyrochlore structures to lead to the large-cell monoclinic structure: we predict 248 Raman active modes. However, such an analysis is only useful if we can correlate it with the high-temperature behavior and phase transformation properties. $Bi_2Hf_2O_7$ was heated to 900 °C (Figure 6) and its Raman spectrum was recorded as a function of temperature. Between 150−250 °C, there was a marked change in the low-frequency region of the spectrum, and the first-order sharp Raman peaks broadened and merged into the broad band at 250−350 cm^{-1} (Figure 7). That result indicates that a dynamic phase transition to a $Bi_2Hf_2O_7$ polymorph of higher symmetry occurs in this temperature range. Such a transformation was not observed by diffraction studies. A transition into an *fcc*-structured phase β-$Bi_2Hf_2O_7$ was only recorded by X-ray diffraction above 450 °C. At that temperature, no significant change in the Raman spectra was observed. It is possible that the $\alpha-\beta$ transition in $Bi_2Hf_2O_7$ occurs first on a local domain scale and is recorded by Raman scattering at $T > 150$ °C before it appears as a global effect that can be observed by diffraction methods at $T > 450$ °C. By 550−600 °C, the spectrum shows even less structure, and the mode located at 525 cm^{-1} has vanished. This correlates well with the structural analysis, which indicates transformation into a body-centered tetragonal structure (γ-$Bi_2Hf_2O_7$) above 600 °C. At 900 °C, the cubic pyrochlore δ-$Bi_2Hf_2O_7$ is formed. However, no further changes were observed in the vibrational spectra upon heating to above ∼600 °C. Subtle changes in the spectra may be partly obscured because of thermal broadening as well as increased second-order scattering. However, it is clear that the major change in local structure is the $\alpha-\beta$ transition. At $T \approx 900$ °C, the weak Raman spectra became overwhelmed by the blackbody radiation that resulted in a rising background to longer wavelengths. The spectral changes were reversed upon cooling, indicating that they corresponded to displacive phase transitions driven by lattice phonon instabilities.

The crystallography shows a sequence of symmetry phase transitions as a function of Hf vs Ti substitution in $Bi_2Hf_{2-x}Ti_xO_7$ analagous to that observed in $Bi_2Hf_2O_7$ with temperature. A similar sequence of effects was observed in the Raman spectra, between monoclinic $Bi_2Hf_2O_7$ and cubic $Bi_2Ti_2O_7$ (Figure 4). There was little change in the spectra between the tetragonal γ- and the cubic δ-phase. The change in the Raman spectra from α-$Bi_2Hf_2O_7$ to the next compound in the sequence was again the most marked change, though interestingly this did not coincide with the phase change in the crystallographic study. The disorder appears in the Raman data as the sharp peaks disappear at lower Ti contents than in the PXD study. Spectra of $Bi_2Ti_2O_7$ were obtained at low temperature (Figure 8). The first-order peaks became sharper and better defined; however, the broad features still remained, even at the lowest temperatures obtained in this study (145

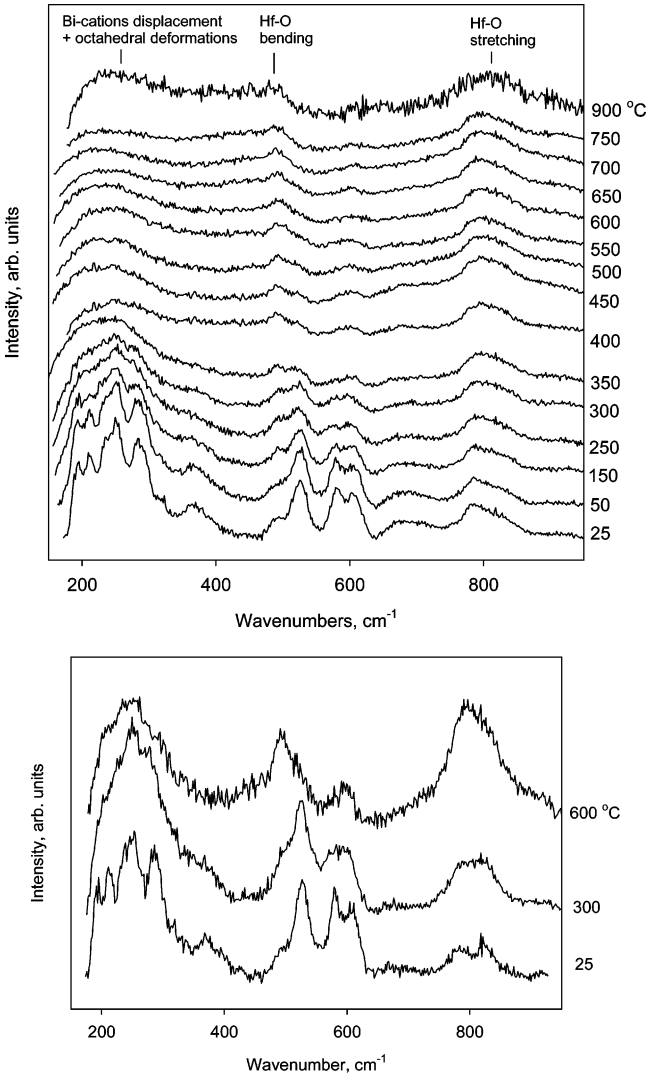

Figure 6. Raman spectra of $Bi_2Hf_2O_7$ collected with increasing (top) and decreasing (bottom) temperature. Temperatures are given in °C.

K). Similar results were observed for $SrTiO_3$ perovskite, below the cubic-tetragonal phase transition at 110 K,[31] which is also consistent with the absence of ordering in $Bi_2Ti_2O_7$ at low temperature as observed by PND.[13]

Discussion

At room temperature, α-$Bi_2Hf_2O_7$ is isostructural with α-$Bi_2Sn_2O_7$. The static displacements of Bi and O′ lead to zigzag Bi−O′ chains with one short (2.196−2.285 Å, average = 2.238 Å) and one long (2.567−2.678 Å, average = 2.628 Å) Bi−O′ bond. The O′−Bi−O′ bond angle, which in a standard pyrochlore would be 180°, varies from 132.69 to 177.28°. The displacement of Bi is more pronounced perpendicular to the O′−O′ axis. This was noted for α-$Bi_2Sn_2O_7$, where displacement in this plane was on average four times that in the direction of the O′−O′ axis.[20] The Hf−O subnetwork is distorted to a lesser extent than that of the Bi−O′. The average Hf−O linkage is 2.090 Å with a range from 2.074 to 2.105 Å. The Hf−O−Hf angles range from 120.0 to 145.6° with an average of 134.0°.

The limited information available for the β-$Bi_2Hf_2O_7$ polymorph at 450 °C indicates transformation to a higher

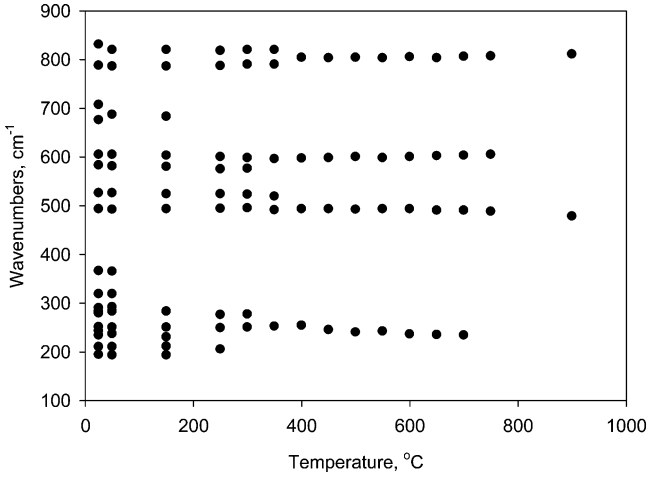

Figure 7. Temperature dependence of Raman shifts measured for $Bi_2Hf_2O_7$.

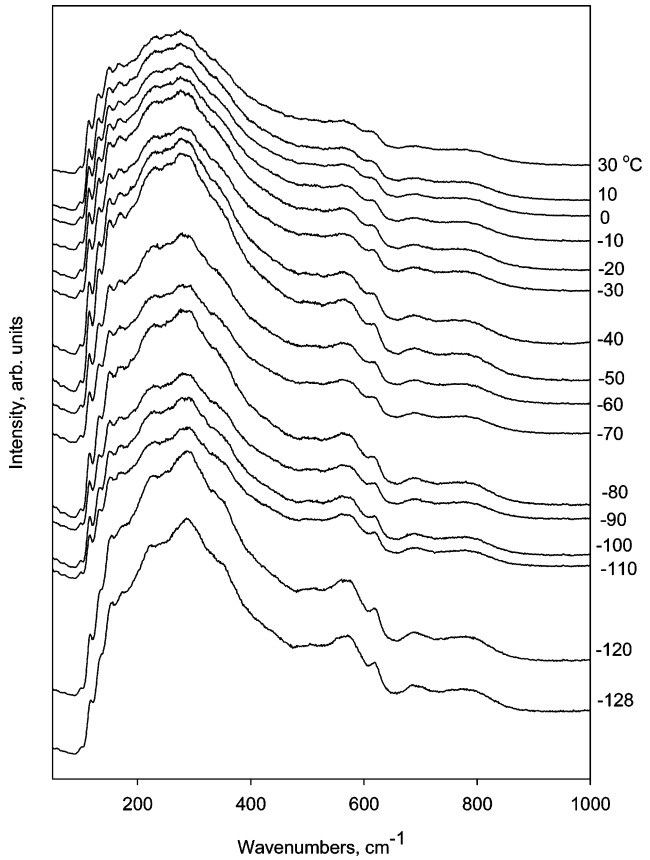

Figure 8. Raman spectra collected from $Bi_2Ti_2O_7$ collected during cooling. Temperatures are given in °C.

symmetry face-centered cubic unit cell with $a = 21.733(2)$ Å occurs. It is reasonable to expect that this phase is less ordered than the α-phase. This may include split bismuth sites, as seen at higher temperatures, with the consequent reduction in local order facilitating relaxation into cubic symmetry.

The compound transforms to a tetragonal γ-$Bi_2Hf_2O_7$ polymorph at 600 °C with smaller cell parameters of $a = 7.68966(3)$ and $c = 10.85169(8)$ Å, again reflecting a reduction in the degree of Bi−O′ ordering. This phase has not been identified in $Bi_2Sn_2O_7$ but offers an insight into the possible mechanism of the phase change behavior of both compounds. Hafnium is bonded to six oxygens with contacts of 2.059, 2.087 and 2.098 Å to form a slightly distorted

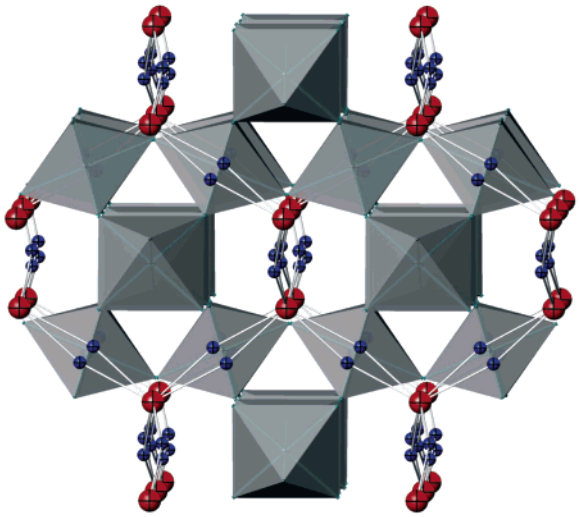

Figure 9. Structure of $Bi_2Hf_2O_7$ at 600 °C highlighting the two-dimensional Bi(blue)−O′(red) zigzag chain within the puckered ring created by the HfO_6 octahedra (gray).

octahedron. The network of these HfO_6 octahedra is close to that of an ideal pyrochlore (Figure 1 and Figure 9) with the familiar puckered O ring and Hf−O−Hf bond angles of 133.7, 136.4, and 134.1°. The scattering density of Bi is positioned toward one-half of this ring, with the next bismuth in the Bi−O′ chain being located toward the opposing half of the next O ring. This gives a Bi−O′ chain that follows a cork-screw formation as it oscillates in both the x and z directions. Where each of the split bismuth sites is associated with one side of the O ring there are two Bi−O contacts to the closest edge (2.329 and 2.644 Å), two to the apical oxygens (2.433 and 3.025 Å), and two to the furthest edge (2.851 and 3.110 Å). The lone pair is presumably positioned in the void created by this arrangement.

At 900 °C, δ-$Bi_2Hf_2O_7$ adopts a more standard cubic pyrochlore unit cell with $a = 10.87791(3)$ Å. The hafnium is surrounded by six O atoms on 48*f* sites ($x = 0.4246$). Anisotropic thermal parameters for these oxygens are consistent with local tilting of the HfO_6 octahedra giving a Hf−O−Hf bond angle of 133.8°. The Hf−O contacts (2.09 Å) are in good agreement with those observed in $La_2Hf_2O_7$ (2.10 Å).[41] The bismuth is displaced away from the −3*m* center of symmetry, normally occupied by *A* cations in ideal pyrochlores, because of the sterically active lone pair. The coordination sphere of bismuth is different depending on whether the 96*g* or 96*h* model is used, Figure 10. Both, however, result in the lone pair of electrons being directed toward a vacant site in the bismuth coordination polyhedron, which may be explained by a mixing of the s and p orbitals on the metal ion.[42] In the 96*g* model, there is one short Bi−O contact of 2.293 Å, two of 2.529 Å, two longer contacts of 2.926 Å, and one very long contact of 3.114 Å. The lone pair is then likely to lie along the direction of this longest distance. The 96*h* model has two contacts of 2.361 Å, two of 2.734 Å, and two of 3.061 Å. The lone pair in this case adopts a position between the two longest Bi−O contacts.

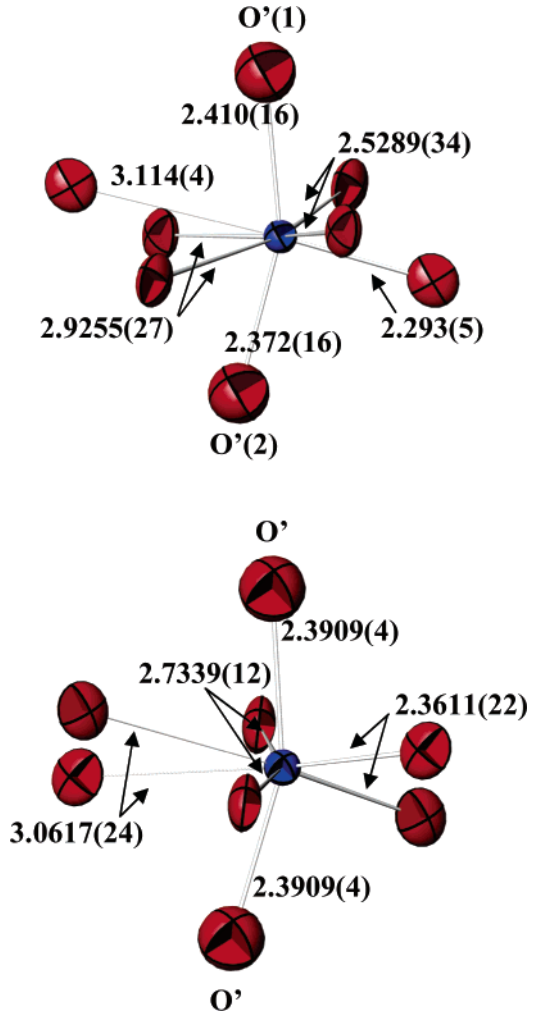

Figure 10. Coordination environment of Bi in $Bi_2Hf_2O_7$ at 900 °C for (top) the 96*g* model and (bottom) the 96*h* model.

The site occupied also affects the Bi−O′ bonding. The 96*g* model leads to bond lengths of 2.372 and 2.410 Å with an O′−Bi−O′ angle of 160.09°, whereas in the 96*h* model, all contacts are at 2.391 Å with an O′-Bi−O′ angle of 160.15°. These differences were also noted for γ-$Bi_2Sn_2O_7$ where, as in this study, it was not possible to distinguish between the two models on the basis of chemical plausibility.

The most interesting feature for comparison between each of the phases is that of the Bi−O′ network. Figure 11 shows the variation in coordination environment about O′. At room temperature, the bismuth and oxygen adopt specific sites, resulting in a variety of bond lengths and angles, with one long (~2.63 Å) and one short (~2.24 Å) contact from Bi to O′. These order throughout the structure with an icelike arrangement in which each O′ has two long and two short Bi−O′ bonds. In the γ-phase, displacements again result in a distortion of the Bi−O′ sublattice. The distortion is, however, less ordered than that of the α-phase, made possible by the increasing energy of the system. In this case, each of the two-fold bismuth sites has bonds of 2.354 and 2.430 Å to O′. Thus, the overall bismuth scattering density occupies a position approximately equidistant from the neighboring oxygens. The accommodation of the bismuth lone pair leads to an O′−Bi−O′ angle of 159.2°. The disorder represented by the split site shows that, at least on the length scale of a

(40) *Molecular Vibrations in Crystals*; Decius, J. C., Hexter, R. M., Eds.; McGraw-Hill: New York, 1977.
(41) Sleight, A. W. *Inorg. Chem.* **1968**, *7*, 1704.
(42) Orgel, L. E. *J. Chem. Soc.* **1959**, 3815.

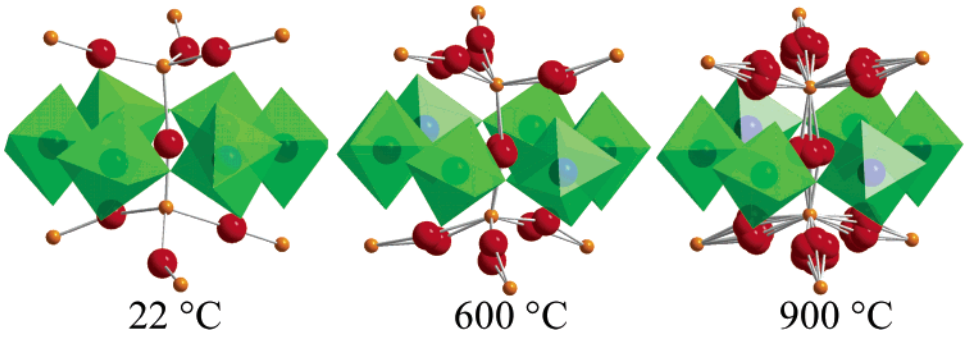

Figure 11. Coordination about O′ at increasing temperature (O′ orange, Bi red, HfO_6 octahedra) in $Bi_2Hf_2O_7$.

diffraction experiment, the icelike lattice is no longer present. At 900 °C the dynamic displacement of the bismuth to form a ring of scattering density allows the lone pair to be accommodated while maintaining a tetrahedral geometry in the O′-O′ network. The O′−Bi−O′ angle of 160.2° to each individual site is close to that of the γ-phase, but is 180° if taken through the center of scattering density. These changes represent the gradual increase in symmetry and disorder with increasing temperature.

Bismuth site displacements in pyrochlores have also been discussed in terms of satisfying the bonding requirements of the Bi atom. For example, the bond valence sum (BVS) of the A site in the BZN composition $(Bi_{0.75}Zn_{0.21})(Nb_{0.75}Zn_{0.25})O_{6.92}$ was found to increase from 2.03 to 2.36 valence units (compared with an ideal value of 2.47 v.u.) as the averaged atomic position was displaced from its ideal site.[3] BVS values were calculated[43] for $Bi_2Hf_2O_7$, comparing the values from the crystal structures described above with those obtained with the Bi atom on its ideal site, centrally placed between the two O′ neighbors. In α-$Bi_2Hf_2O_7$, an averaged BVS of 2.32 v.u. was obtained with centered bismuth atoms and increased to 2.94 v.u. when the atom was displaced to its final position. In the γ-phase, the displacements caused an increase from 2.12 to 2.38 v.u. In δ-$Bi_2Hf_2O_7$, the BVS of 2.145 v.u. increased to 2.38 v.u. with displacement to a 96*g* position and to 2.37 v.u. when the 96*h* was used (as stated previously, these were indistinguishable crystallographically).

The incorporation of titanium into the hafnium sublattice leads to a unit cell contraction as would be expected from the smaller ionic size of Ti^{4+} (60.5 pm) compared with Hf^{4+} (71 pm).[44] This can be observed by viewing plots of the variation in lattice parameters (Figure 12) and cell volume (Figure 13) with composition, normalized to a normal (∼10 Å) pyrochlore cell for clarity. The expected linear trend in volume with compositional variation is not strictly observed; this may imply some compositional inhomogeneity within samples. It is clear that larger B cations lead to ordering of the Bi displacements in this system; Hf^{4+} is actually slightly larger than Sn^{4+} (69 pm). Indeed, with Zr^{4+} (72 pm), the pyrochlore type structures are not stable.[21] It appears that a larger B-cation results in the Bi^{3+} lone pair being unable to be accommodated within puckered ring, hence Bi moves toward one of the O′ atoms. Ordering can then result from

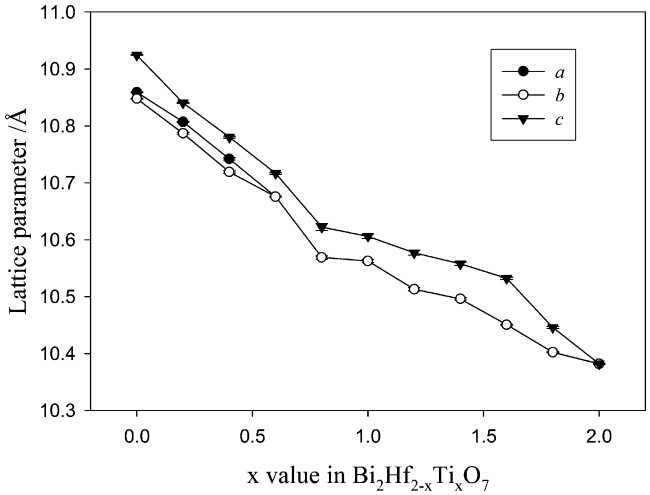

Figure 12. Variation of lattice parameters of the $Bi_2Hf_{2-x}Ti_xO_7$ series with *x*. Distances are normalized to a normal pyrochlore type for clarity.

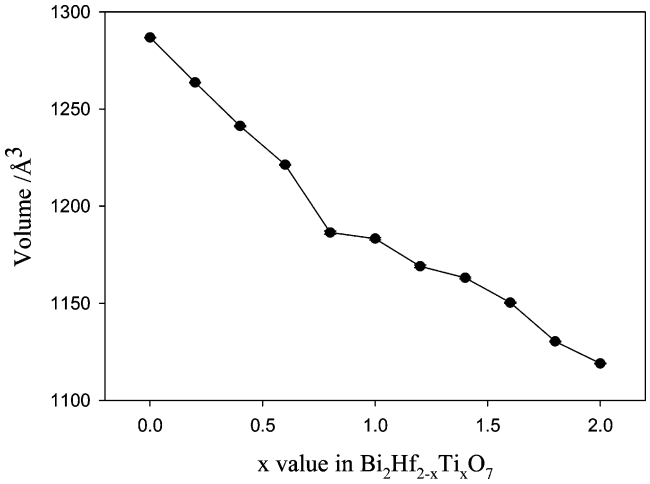

Figure 13. Variation in cell volume of the $Bi_2Hf_{2-x}Ti_xO_7$ series with *x*. Volumes are normalized to a normal pyrochlore type for clarity.

the need to balance charges between O′ atoms, hence each taking two long and two short Bi−O′ bonds. The Bi displacements in $Bi_2Ti_2O_7$ are already large compared with isostructural phases such as BZN or $Bi_2Ru_2O_7$,[13] so it is unsurprising that some displacement toward one of the O′ atoms occurs even in $Bi_2Hf_{0.2}Ti_{1.8}O_7$, resulting in the tetragonal phase. Equally, it might be expected that relieving the pressure on the puckered ring of O atoms around Bi by heating $Bi_2Hf_2O_7$ and expanding the lattice would have an effect similar to reducing the effective size of the B cations by substituting Hf with Ti.

(43) Brese, N. E.; O'Keeffe, M. *Acta Crystallogr., Sect. B* **1991**, *47*, 192.
(44) Shannon, R. D. *Acta Crystallogr., Sect. A* **1976**, *32*, 751.

The major finding from the Raman spectra is that the most significant change in local structure is from α-$Bi_2Hf_2O_7$ to the next structure in the series, whether this is the doubled cubic β-$Bi_2Hf_2O_7$ or the tetragonal γ-type $Bi_2Hf_{1.4}Ti_{0.6}O_7$. This suggests that the local structure of the α-phase is more differentiated from the other three phase types. This is likely to mean that the ordered icelike network is destroyed at the first phase change, implying that it is not present in the β-$Bi_2Hf_2O_7$ structure. In the α-phase, there are two types of ordering present, (a) the ordered long and short Bi−O′ bonds resulting in an icelike network and (b) the direction of the Bi displacement perpendicular to O′−O′ resulting in a corkscrew effect. The first may be lost in the α−β transition, whereas the second progressively becomes more disordered in the $\beta-\gamma$ and $\gamma-\delta$. Confirmation of this will require a full structure solution of β-$Bi_2Hf_2O_7$, or maybe more likely β-$Bi_2Sn_2O_7$, where the temperature stability means that higher sintering temperatures can be used, resulting in lower diffraction linewidths.

Conclusions

The structural behavior of $Bi_2Hf_2O_7$ has been determined by variable temperature neutron and X-ray diffraction. Four distinct phases were observed, which represent a gradual increase in symmetry and disorder with temperature. Three of these have previously been observed in $Bi_2Sn_2O_7$. The driving force for these changes is the need to accommodate the active bismuth lone pair in a space that is being compressed by the large Hf^{4+} cation. A similar trend is observed with increasing titanium substitution for hafnium in the series $Bi_2Hf_{2-x}Ti_xO_7$. Raman spectra show that α-$Bi_2Hf_2O_7$ has a local structure that is very different from the other three phases, suggesting that the icelike Bi^{3+} site ordering is present only in this α-phase and providing clues about the structure of the unsolved β-phase in bismuth stannate and hafnate.

Acknowledgment. The authors thank the Royal Society for a University Research Fellowship (A.L.H.), EPSRC for a studentship (S.J.H.), and support through a Portfolio award that supports the vibrational spectroscopy (P.F.M. and O.S.). PFM also acknowledges an EPSRC Senior Fellowship and a Wolfson-Royal Society Research Merit Award. CCLRC provided beam time at ISIS on grant RB20146 and Dr R. I. Ibberson is thanked for assistance with the PND data collection. Thanks also to Dr E. Bailey for attempting warm pressing of samples for dielectric measurements.

Supporting Information Available: Crystallographic information files (CIF) with embedded PND data for the α-, γ- and δ-$Bi_2Hf_2O_7$ structures. This material is available free of charge via the Internet at http://pubs.acs.org.

CM062864A